ROTATION INVERSIONS OF ARTIFICIAL SOLARFLAG SUN-AS-A-STAR DATA

W. J. Chaplin,[1] T. Sekii[2], T. Appourchaux[3], F. Baudin[3], P. Boumier[3], T. Corbard[4], A. Eff-Darwich[5],
Y. Elsworth[1], S. T. Fletcher[1], E. Fossat[6], R. A. García[7], A. Jiménez[5], S. J. Jiménez-Reyes[5], M. Lazrek[8,6,4],
J. W. Leibacher[9], J. Lochard[3], R. New[10], P. Pallé[5], C. Régulo[5,11], D. Salabert[9], N. Seghouani[12], T. Toutain[1,13] and
R. Wachter[14]

[1]School of Physics and Astronomy, University of Birmingham, Edgbaston, Birmingham, B15 2TT, U.K.
[2]Solar and Plasma Astrophysics Division and Solar-B Project Office, National Astronomical Observatory of Japan,
Natural Institutes of Natural Sciences, Mitaka, Tokyo 181-8588, Japan
[3] Institut d'Astrophysique Spatiale (IAS), Batiment 121, F-91405, Orsay, France; Université Paris-Sud 11 and CNRS
(UMR) 8617
[4]Laboratoire Cassiopée, UMR OCA-CNRS 6202, Observatoire de la Côte d'Azur, F-06304 Nice, France
[5] Instituto de astrofísica de Canarias, 38205, La Laguna, Tenerife, Spain
[6] LUAN, UMR 6525, Université de Nice-Sophia Antipolis, 06108 Nice Cedex 2, France
[7] Service d'Astrophysique, CEA/DSM/DAPNIA, CE Saclay, 91191 Gif sur Yvette, France
[8] LPHEA, Faculte des Sciences Semlalia, Universite Cadi Ayyad, Marrakech, Morocco
[9]National Solar Observatory, 950 North Cherry Avenue, Tucson, AZ 85719
[10] Faculty of Arts, Computing, Engineering and Sciences, Sheffield Hallam University, Sheffield S1 1WB
[11] Dpto. de Astrofsica, Universidad de La Laguna, La Laguna, 38206, Tenerife, Spain
[12] CRAAG, BP63, Bouzareah, Alger, Algeria
[13] Institute of Theoretical Astrophysics, University of Oslo, P.O. Box 1029, N-0315 Oslo, Norway
[14] W. W. Hansen Experimental Physics Laboratory, Stanford University, Stanford, CA 94305-4085

solarFLAG URL http://bison.ph.bham.ac.uk/˜wjc/Research/FLAG.html

ABSTRACT

We report on results of rotation inversions using as input fitted splitting estimates from the first solar Fitting at Low-Angular degree Group (solar FLAG) hare-and-hounds exercise. The 'hounds in the group fitted an artificial 9.5-yr dataset made by the 'hare to mimic full-disc Doppler velocity observations of the Sun.

Key words: Sun: helioseismology – Methods: data analysis.

1. INTRODUCTION

In Chaplin et al. (2006), we reported on results of the first solarFLAG hare and hounds exercise. Artificial Sun-as-a-star data, spanning 3456 simulated days – a length roughly commensurate to one 11-year cycle of solar activity – were generated by WJC (the 'hare'), with a S/N per unit time characteristic of that in the GOLF and Bi-SON Doppler velocity data. In one timeseries the mode parameters were unchanged in simulated time (the 'stationary' set); in the other, they were varied to mimic the effects of the solar cycle ('cycle' set). These solarFLAG timeseries were made available, with 100-per-cent duty cycles, for the nine hounds to analyze (TA, FB, STF,

RAG, SJJ-R, ML, DS, TT and RW). Estimates of the fitted splittings were returned to the hare for subsequent analysis. In the Sun-as-a-star data, it is the prominent outer components of the multiplets that dominate the fitting, and so the fitted splittings are close to the sectoral mode splittings:

$$\delta\nu_s(l,n) = \frac{[\nu_{l,n,m=l} - \nu_{l,n,m=-l}]}{2l}. \qquad (1)$$

For each hound, splitting results from the two sets were found to agree to well within the fitting uncertainties. In spite of this good agreement, when the splittings of the hounds were compared with one another (for each of the 'cycle' and 'stationary' data) significant differences were uncovered at $l = 2$ and 3. These splitting differences are apparent in Fig. 1, which shows the fitted splittings of all the hounds given by analysis of the stationary set (one curve for each hound). Evidence was presented in Chaplin et al. that suggests this unwanted bias had its origins in several effects. The most important came from the different way in which the hounds modeled the visibility ratio of the different rotationally split components. In summary, the results suggested that accurate modeling of the ratios is vital to avoid the introduction of significant bias in the estimated splittings.

In this paper, we discuss results of inverting the splittings that each hounds obtained from analyzing the stationary solarFLAG dataset. With only these 'sectoral-like' mode
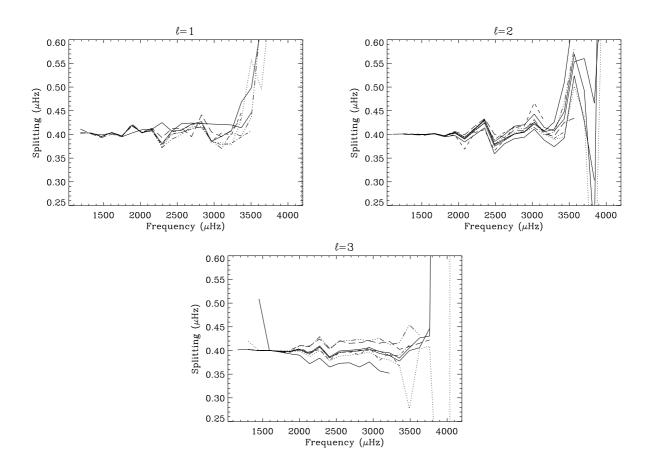
Figure 1. Fitted splitting results of the hounds.

splittings available, one cannot investigate the latitudinal variation of the rotation. Therefore, one has to simplify the inverse problem to one that is radial only. Since the amplitudes of the sectoral modes are concentrated near the equator of the Sun, one might consider regarding the task as an investigation of the radial variation of rotation in the equatorial plane. However, the degree of concentration near the equator depends on l. This means that the sectoral splittings are contaminated by the latitudinally varying component of rotation by an amount that depends on l, rendering it difficult to obtain results that are easy to interpret. Clearly, this is an important issue for real data; we touch on this in Appendix A. However, here we have obviated this issue by using artificial data computed from a model of the Sun that rotates with a latitudinally invariant angular velocity (and one for which all synodic splittings are $0.4\,\mu$Hz).

Here, we have also included for the inversions the fitting results of the hare, WJC, giving ten low-l splitting sets in all. We augmented the low-l splitting sets of each of the hounds with higher-degree data, borrowing their properties from a 144-d MDI dataset (Schou et al. 1998). The additional data comprise the 1630 mode splittings between $l = 4$ and $l = 250$ that exist in the MDI set. All splittings were fixed at $0.4\,\mu$Hz, and the associated uncertainties were taken to be the error estimates of the MDI a_1 coefficients. We added no random errors to the 'MDI' splittings.

2. 'ROTATION' INVERSIONS

As was stated above, we consider a one-dimensional problem. According to linear perturbation theory, the observed splitting, $\Delta\nu_{nl}$, of a multiplet of degree l and radial order n, whose observational error is e_{nl}, is related to the rotation rate Ω, considered to be a function of only the radial coordinate r, via the following integral:

$$\Delta\nu_{nl} = \int_0^R K_{nl}(r)\Omega(r)\mathrm{d}r + e_{nl} , \qquad (2)$$

where R is the solar radius. (Throughout this paper Ω is, unconventionally, the rotation rate – measured in nHz – and not the angular velocity of the model Sun.) The function $K_{nl}(r)$ is called the splitting kernel, and is calculated from a solar model and the displacement eigenfunctions associated with the mode.

In computing the splitting kernel, we neglect the Coriolis force, rendering that kernel unimodular: i.e.,

$$\int_0^R K_{nl}(r)\mathrm{d}r = 1 . \qquad (3)$$

We do this in order to make it easier to relate $\Omega(r)$ with the fitted splitting frequencies (this has little detrimental effect on what we are investigating). In particular, a uniform rotation rate of $0.4\,\mu$Hz leads to a uniform true splitting of $0.4\,\mu$Hz.

In the inverse rotation problem one aims to use a set of integral constraints – in the form of equation (2) – to infer $\Omega(r)$. Of the several techniques that are available, we have chosen to use the optimally localized averaging (OLA) introduced by Backus and Gilbert (1968, 1970), in a form which we now explain (and as described in Chaplin et al. 2004a).

We construct a linear combination of the $\Delta\nu_{nl}$ to obtain an estimate of $\Omega(r)$. An estimate $\hat{\Omega}(r_j)$ aimed at being centred about some target radius r_j is then simply a weighted average of $\Delta\nu_{nl}$:

$$\hat{\Omega}(r_j) = \sum_{nl} c_{nl}(r_j)\Delta\nu_{nl} ; \qquad (4)$$

the weighting factors $c_{nl}(r_j)$ are called inversion coefficients, which in this simplified exercise satisfy $\sum c_{nl} = 1$. From relation (2) it follows that

$$\hat{\Omega}(r_j) = \int_0^R K(r;r_j)\Omega(r)dr + \sum_{nl} c_{nl}(r_j)e_{nl} , \qquad (5)$$

where

$$K(r;r_j) \equiv \sum_{nl} c_{nl}(r_j)K_{nl}(r) , \qquad (6)$$

which we constrain to be unimodular:

$$\int_0^R K(r;r_j)\mathrm{d}r = 1 , \qquad (7)$$

rendering the estimate $\hat{\Omega}(r_j)$ essentially an average of $\Omega(r)$ weighted by the 'averaging kernel' K. Indeed, were the data errors to be unbiased, the statistical expectation of the error in $\hat{\Omega}(r_j)$ would vanish, and the statistical expectation of $\hat{\Omega}$ would be precisely that average. Ideally, the averaging kernel should have a sharp peak at $r = r_j$ without any negative sidelobes, for then one could consider $\hat{\Omega}$ to be a pointwise estimate of $\Omega(\bar{r})$, where $\bar{r} \simeq r_j$ is the centre of K. In attempting to achieve this property one introduces a measure S of the spread of the averaging kernel, which one might try to minimize. The measure we use here is

$$S = \int_0^R K(r;r_j)^2(\tau - \tau_j)^2\mathrm{d}r , \qquad (8)$$

where

$$\tau(r) \equiv \int_0^r \frac{\mathrm{d}r}{c} \qquad (9)$$

is the acoustic radius and $\tau_j = \tau(r_j)$. However, too sharp a localization of K leads to a large magnification of the data errors, and therefore it has to be penalized in the procedure.

Accordingly, for a given target point we determine the inversion coefficients by minimizing $S + \alpha V$ for some positive parameter α, subject to the unimodular condition $\sum c_{nl} = 1$, where

$$V = \sum_{nl} c_{nl}(r_j)^2\sigma_{nl}^2 \qquad (10)$$

is the formal variance of $\hat{\Omega}(r_j)$, under the assumption that the data errors are independent, yielding an error covariance matrix of the form

$$\mathrm{cov}[\Delta\nu_{nl}, \Delta\nu_{n'l'}] = \langle e_{nl}e_{n'l'}\rangle = \sigma_{nl}^2 \delta_{nn'}\delta_{ll'} \ . \quad (11)$$

The trade-off parameter α determines the balance between localization and error magnification, and is chosen at will. From the inversion coefficients an estimate of the rotation rate and its formal error $\sqrt{V}$ are evaluated according to formulae (5) and (10). The centre of the averaging kernel, $\bar{r}$, and its width, w, are estimated according to the original Backus-Gilbert prescription, save that the width is scaled by a factor β chosen such that w would correspond to the FWHM were the averaging kernel to be a Gaussian function. Thus

$$\bar{r} = A_1/A_0 \ , \quad (12)$$
$$w = 12(A_2 - A_1\bar{r})\beta, \quad (13)$$

where $\beta = 2\sqrt{2\pi\ln 2}/3 \simeq 1.4$, and

$$A_k = \int_0^R r^k K(r; r_1)^2 \mathrm{d}r \ . \quad (14)$$

The width w is essentially proportional to the spread S, and would be precisely so if the acoustic radii were replaced by geometrical radii in equation (8). One can redefine the quantities for consistency, but generally the differences are small because the averaging kernels are quite well localized.

3. RESULTS

Fig. 2 shows estimates of the rotation rate of the artificial Sun given by inversion of each of the ten (MDI-augmented) sets of low-l splittings (one curve per hound). We recall from above that in Chaplin et al. (2006) some disagreement was found between the fitted splittings of the hounds when the hounds 'chose' their own m-component height ratios for the fitting. The results in Fig. 2 come from these initial sets of splittings. A typical result for one of the hounds is shown in Fig. 3, which plots the estimated rotation given by inversion of the augmented splitting set of WJC.

The general trend of the inversion results is toward overestimation of the actual rotation rate in the core. This is a consequence of the tendency of the peak-bagging procedures to overestimate the input splittings of the higher-frequency modes (e.g., Appourchaux et al. 2000; Chaplin et al. 2001). The mode peaks are wide in comparison to the splittings in that part of the spectrum, making determination of the frequency splittings difficult.

To give an idea of the significance of the differences between hounds shown in Fig. 2, we have subtracted from each estimated rotation rate the correct value of $0.4\,\mu\mathrm{Hz}$, and then normalized the difference by the mean formal uncertainty of all the hounds' inversions at that target radius. The resulting residuals are plotted, in units of the formal inversion uncertainty, in Fig. 4. The upper panel shows results for which the *full* inversion uncertainties were used. By full, we mean that uncertainties on the splittings of both the low-l solarFLAG and the higher-l 'MDI' data were propagated to give the formal inversion uncertainties. In the lower panel, we show results where the inversion uncertainties were instead given by propagation of *just* the splitting uncertainties on the low-l data. Because all MDI splittings were fixed at $0.4\,\mu\mathrm{Hz}$, the only real scatter comes from the solarFLAG data: this second set of residuals allows therefore for a direct assessment of the low-l-only contributions, and the extent of any internal disagreement between hounds, throughout the interior. On the other hand the analysis made with the full uncertainties tells us (amongst other things) how the scatter will be diluted when the solarFLAG data are augmented by the higher-degree modes.

Fig. 5 shows the RMS of the residuals plotted in Fig. 4: the solid curve was calculated from the residuals in the upper panel of Fig. 4 (full inversion uncertainties); while the dashed curve was made from the data in the lower panel of Fig. 4 (low-l-only inversion uncertainties)

The results in the lower and upper panels of Fig. 4 are similar in the core: there, the inversion uncertainties are dominated by the splitting uncertainties of the low-l modes. However, beyond the core the higher-l data carry much greater weight, and the full inversion uncertainties are several times larger than those determined by the low-l data only. This is why the significance of differences between the residuals (curves) is higher in the residuals made using only the low-l uncertainties.

The results show that in the core there is disagreement between the estimated rates of rotation, disagreement that, at its most extreme, is several times larger than the inversion uncertainty. The RMS curves in Fig. 5 give a measure of the size of this additional uncertainty. We remind the reader that it is present on top of the general trend of the results toward overestimation of the rotation rate in the core. The rate is overestimated in the core by about 1σ on average (Fig. 4).

The solid RMS curve in Fig. 5 – calculated with the full inversion uncertainties – shows the presence of scatter at a level over and above the notional, formal, 1σ level. At radii beyond $\sim 0.3\,r/R_\odot$, little scatter is seen, and the curves agree to within a fraction of 1σ. In contrast, residuals determined using the low-l-only inversion uncertainties (lower panel of Fig. 4, dashed curve in Fig. 5) show notable disagreement at several locations throughout the interior. Of particular note is the extra dispersion present just below $r/R_\odot \sim 0.6$, and also much closer to the surface. It is possible that this is where the solarFLAG modes were used to eliminate contributions from the higher-l MDI modes in the deep interior.
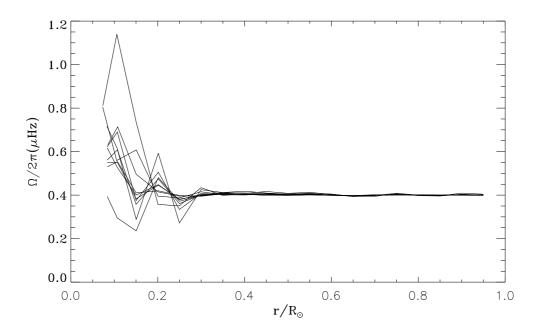
Figure 2. Estimates of the rotation rate of the artificial Sun given by inversion of each of the ten (augmented) sets of splittings (one curve per hound). The input data come from fits in which the hounds made their own choice over what sizes of m-component height ratio to use in the fitting.
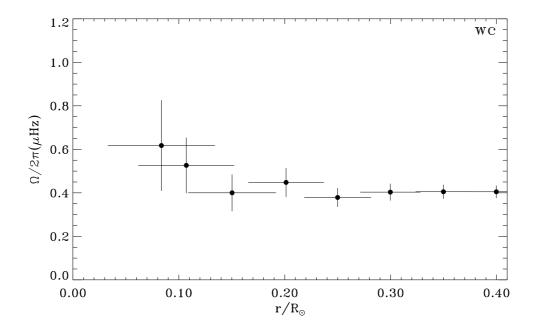

Figure 3. Estimates of the rotation rate of the artificial Sun given by inversion of the (augmented) splitting set of WJC.
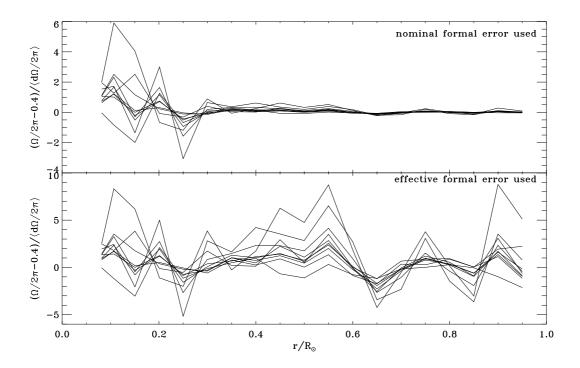
Figure 4. *Difference between estimated rotation rate and the correct value of* $0.4\,\mu$Hz, *normalized by the formal uncertainty of the inversion at that target radius. Upper panel: inversion uncertainties calculated from the* full *splitting set, i.e., both the low-l solarFLAG and higher-l 'MDI' splitting uncertainties. Lower panel: inversion uncertainties calculated from the low-l splitting uncertainties only.*
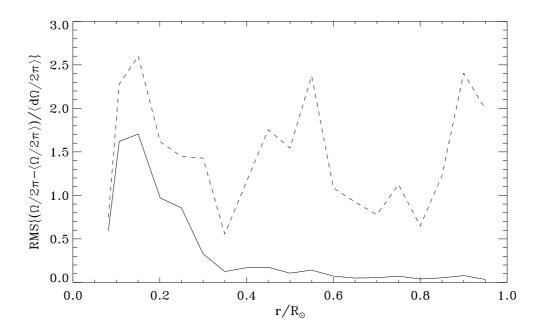

Figure 5. RMS *of the residuals plotted in Fig. 4. Solid line:* RMS *difference for residuals calculated with* full *inversion uncertainties. Dashed line:* RMS *difference for residuals calculated with low-l-only inversion uncertainties.*

REFERENCES

[1] Appourchaux T., Chang H-. Y., Gough D. O. & Sekii T., 2000, MNRAS, 319, 365

[2] Backus G. & Gilbert F., 1968, Geophys. J. Roy. Astron. Soc., 16, 169

[3] Backus G. & Gilbert F., 1970, Phil. Trans. Roy. Soc. London, Ser. A, 266, 123

[4] Chaplin W. J., Elsworth Y., Isaak G. R., Marchenkov K. I., Miller B. A., New R., 2001, MNRAS, 327, 1127

[5] Chaplin W. J., Elsworth Y., Isaak G. R., Miller B. A., New R., Thiery S., Boumier P., Gabriel A. H., 2003a, MNRAS, 343, 343

[6] Chaplin W. J., Sekii T., Elsworth Y., Gough D. O., 2004a, MNRAS, 355, 535

[7] Chaplin W. J., Appourchaux T., Elsworth Y., Isaak G. R., Miller B. A., New R., 2004b, A&A, 424, 713

[8] Chaplin W. J., et al., 2006, MNRAS, 369, 985

[9] Corbard T., Di Mauro M. P., Sekii T., and the GOLF team, 1998, in: Proc. SOHO6/GONG98 'Structure and Dynamics of the Sun and Sun-like Stars', ESA SP-418, p. 741

[10] García R. A., Corbard T., et al., 2004, SolPhys, 220, 269

[11] Ritzwoller M. H., Lavely E. M., 1991, ApJ, 369, 557

[12] Schou J. et al., 1998, ApJ, 505, 390

A. EFFECT OF HEIGHT RATIO SENSITIVITY ON A-COEFFICIENT CONTENT OF SUN-AS-A-STAR SPLITTINGS

Frequencies from the resolved-Sun observations are usually described using a polynomial expansion of the form:

$$\nu_{n,l,m} = \nu_{n,l}^{\mathrm{RES}} + \sum_{j=1}^{j_{\max}} a_j(n,l) \, l \, \mathcal{P}_l^j(m). \qquad (15)$$

where $\nu_{n,l}^{\mathrm{RES}}$ is the centroid frequency of the multiplet, $j_{\max} \leq 2l$, and the basis functions are polynomials related to Clebsch-Gordan coefficients (Ritzwoller & Lavely 1991). A clean 1D inversion in radius can be made by inversion of the a_1 coefficients. However, some of the Sun-as-a-star splittings have contributions from a_3 and a_5, making use of the Sun-as-a-star splittings problematical. One approach is to attempt to correct the Sun-as-a-star values for the contributions of the a_3 and a_5, in an attempt to give some proxy for the 'clean' a_1 (e.g., see Corbard et al. 1998; García et al., 2004). Here, we show that the correction is uncertain at $l = 3$, because of the presence of the $m = 1$ components.

We begin by expressing the Sun-as-a-star splittings in terms of the odd-a coefficients. At $l = 1$ only the sectoral components are observed in the Sun-as-a-star data, and so we have (using the format of Equation 1):

$$\delta\nu_s(1,n) = \frac{[\nu_{1,n,1} - \nu_{1,n,-1}]}{2} = a_1(n,1). \qquad (16)$$

At $l = 2$ the relationship is in principle a straightforward one. This is because, even though the $m = 0$ component is also observed, its position in frequency with respect to the sectoral components, and the centroid, does not depend on the odd-a coefficients. We therefore have:

$$\delta\nu_s(2,n) = \frac{[\nu_{2,n,2} - \nu_{2,n,-2}]}{4} = a_1(n,2) + a_3(n,2). \qquad (17)$$

However, we know in practice that incorrect modelling of the relative visibility of the $m = 0$ and $|m| = 2$ components does have some influence on the fitted value of the splitting: the central component does have a rôle to play.

Matters are much less straightforward at $l = 3$. Here, the $|m| = 1$ components are also observed, albeit at a less prominent level than their sectoral counterparts. There are therefore *two* sets of splittings in play: one between the $|m| = 1$ peaks; and one between the $|m| = 3$. The appropriate splitting to consider for each combination is:

$$\frac{[\nu_{3,n,m} - \nu_{3,n,-m}]}{2m}.$$

We then have

$$\frac{[\nu_{3,n,3} - \nu_{3,n,-3}]}{6} = a_1(n,3) + a_3(n,3) + a_5(n,3), \qquad (18)$$

and

$$\frac{[\nu_{3,n,1} - \nu_{3,n,-1}]}{2} = a_1(n,3) - 3a_3(n,3) + 15a_5(n,3). \qquad (19)$$

Application of the usual Sun-as-a-star fitting strategy imposes an equal frequency splitting between all components. We might therefore expect the fitted $l = 3$ splitting to be some linear combination of the splittings in Equations 18 and 19, with the former, sectoral value receiving much greater weight (because it components appear more prominently in the power spectrum). Let ρ be a simple coefficient that fixes the proportion of each splitting in the final, fitted splitting. We may then write the fitted splitting as:

$$\delta\nu_s(3,n) = (1-\rho)\frac{[\nu_{3,n,3} - \nu_{3,n,-3}]}{6}$$

$$+ \rho\frac{[\nu_{3,n,1} - \nu_{3,n,-1}]}{2}. \qquad (20)$$

Expressed in terms of the odd-a coefficients, the fitted splitting is then:

$$\delta\nu_s(3,n) = a_1(n,3) + (2\rho+1)a_3(n,3) + (14\rho+1)a_5(n,3). \qquad (21)$$

In the absence of the $|m| = 1$ components, i.e., for $\rho = 0$, the fitted splitting would be just $a_1 + a_3 + a_5$. Equation 21 shows that in practice, the influence of the inner components means the contribution of a_3 and a_5 is different in the final splitting. If we assume the coefficient ρ has similar size to that determined for the frequency parameter (Chaplin et al. 2004b) – giving $\rho \approx 0.06$ – we would have a final splitting of $a_1 + 0.76a_3 + 1.84a_5$.

Not only will the effect be determined by the underlying visibility of the various components but the results of Chaplin et al. (2006), on the solarFLAG hare-and-hounds splittings (Fig. 1), suggest that assumptions made in the fitting about the visibility may also have a rôle the play.